An Appraisal of High Resolution Scanning Electron Microscopy Applied To Porous Materials

Sam M. Stevens[†,††], Kjell Jansson[†], Changhong Xiao[†], Shunsuke Asahina[†††], Miia Klingstedt[†], Daniel Grüner[†], Yasuhiro Sakamoto[†], Keiichi Miyasaka[†,††††], Pablo Cubillas[††], Rhea Brent[††], Lu Han[†,†††††], Shunai Che[†††††], Ryong Ryoo[††††], Dongyuan Zhao[†††††], Mike Anderson[††], Ferdi Schüth[†††††], and Osamu Terasaki[†,††††]*

[†] **Department of Physical, Inorganic & Structural Chemistry, Arrhenius Laboratory, Stockholm University**
[††] **The University of Manchester**
[†††] **JEOL Europe**
[††††] **Korea Advanced Institute of Science and Technology**
[†††††] **Shanghai Jiao Tong University**
[†††††] **Fudan University**
[†††††] **Max Planck Institute Mülheim**

Nanoporous materials such as zeolites and mesoporous silica crystals have attracted a lot of attention in recent years. In particular, the incorporation of various materials such as organic molecules, or metal nanoparticles and other inorganic compounds within their pores which give rise to fascinating new functions. For such materials, it is essential to determine their structure, composition and mechanisms of growth in order to maximize their utility in future applications.

Recent progress in the performance of SEM is enormous, especially in low energy imaging where we can now directly observe fine surface structures of porous materials even those that are electrical insulators. Furthermore, by precise filtration and detection of emitted electrons by their energy, we can selectively obtain different types of information such as material composition, location of particles inside or outside the pores etc. The physical processes and technologies behind this precise tuning of landing and detection energies for both impact and emitted electrons, respectively, are explained and illustrated using a number of porous materials including zeolite LTA, SBA-15, SBA-16, zeolite LTL, FDU-16 and Au@TiO_2 ' rattle spheres,' along with comparisons with other techniques such as atomic force microscopy (AFM) and transmission electron microscopy (TEM). We conclude that, by using extremely low landing energies, advanced sample preparation techniques and through a thorough understanding of the physical processes involved, HRSEM is providing new and unique information and perspectives on these industrially important materials.

Introduction

In this report, we classify porous materials based on structural characteristics into the following three categories: (i) Materials with a periodic pore arrangement with uniform size either in periodic framework structures such as microporous zeolites or in amorphous silica wall forming "cavity crystals" such as meso- and macro-porous silica crystals; (ii) Materials which have irregular size of pores in a random arrangement such as mesoporous silica with worm-like pores or random pores in size and arrangement; and (iii) Hollow nano spheres with or without nano-particles inside. Both nanoporous (micro-, meso- and macro-porous) materials and their composites with nano-particles have been prepared. All of these materials are extremely important in a number of different industries. In (i), pores often provide acidic sites and large surface areas for heterogenous catalysis to occur as is the case for (ii) where pores may also be modified with transition metals or used to reversibly bind molecules for medicinal applications. Owing to their porosity and structure it is even possible to use them for both tissue engineering and drug delivery. In the case of (iii), hollow spheres with nanoparticles have also been synthesized with the purpose of maintaining characteristic features of the nanoparticles whilst preventing their aggregation at catalytically active conditions. They also exhibit new properties with their encapsulating hollow spheres. In order to maximize both the efficiency and range of applications of these porous crystals, an understanding of their structure and growth mechanism is therefore extremely important for further control of growth processes to tailor these materials for our specific needs. Such properties we wish to control include, but are not limited to, pore size, level of exposure of pores to the crystal surface, orientation of pores with respect to crystal surface, crystal size and shape, hydrophobicity/hydrophilicity and properties of the guest material.

With regards to porous crystals, scanning electron microscopy (SEM) has long been used as a method to rapidly gather information such as the size and shape of crystals. This is because the microscopes have a large depth of focus and are relatively easy to operate with a minimum of tuition. As visualisation of crystals occurs at scan speeds and at a range of magnifications it is therefore possible to gather a statistically significant amount of data. This information is important when discussing crystal growth trends [1], but does not supply information to scientists about the crystal formation and structural chemistry at the nanometer scale*. Such information may be found from observation of fine surface structure, for example: in zeolite LTA the height and shape of surface terraces, observed by atomic force microscopy (AFM), provides evidence of the existence of discrete growth units from which the crystals form and the nature of the growth mechanism as a function of reaction conditions [2]. In scientific reports of this nature, SEM images usually appear as little more than supporting information or visual expatiation [3] to the scientific observations and discussions on crystal growth as gleaned from other analytical techniques such as atomic force microscopy (AFM) and also by powder X-ray diffraction (XRD), transmission electron microscopy (TEM) and others.

In the last decade there has been a quantum leap forward in the utility of SEM, which we now dub high-resolution SEM (HRSEM). Particular advances include: Improvement of objective lens with smaller chromatic and spherical aberration coefficients; precise control of the landing energy of impact electrons and therefore a dramatic reduction in charging (the main contributor to loss of information in observation of insulating materials) whilst retaining a suitably small probe size; and an ability to obtain selective information by tuning proper electron energy ranges and collecting angles for detection. Important crystal features, such as mesoporous channel openings, terminations and curvature [4] and other surface features such as twinning and growth fronts in zeolites [5] have been reported.

We begin by comparing the level of detail and various other merits between HRSEM and AFM, then further quantify the measurable level of surface topography and show that the HRSEM is able to identify nanometer scale crystal surface features through an elegant example, whilst at the same time providing information on larger crystal details - both with a high level of fidelity. We then show that through new sample preparation techniques, the detail HRSEM can reach is

*That said, SEM is also able to determine the chemical composition of points on a crystal by measuring the energy / wavelength of the characteristic X-ray in energy / wavelength dispersive spectroscopy (EDS / WDS), respectively but the elemental information is an average over the range of a micrometer.

[†]SE-10691 Stockholm, Sweden, terasaki@struc.su.se

[††††]Daejeon 305-701, Korea, terasaki@kaist.ac.kr

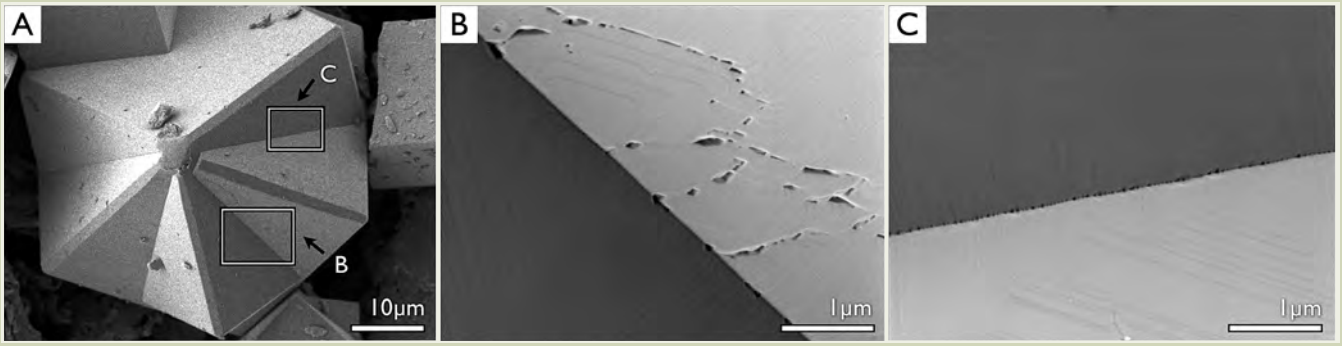

Fig.1 HRSEM images of twinned crystals of zeolite LTA. (B) and (C) show the interface between the two twins located in the boxes on (A). 1 keV landing energy, 2.5 keV column energy. In-lens detector, Sb mode (See Figure 8-1, D).

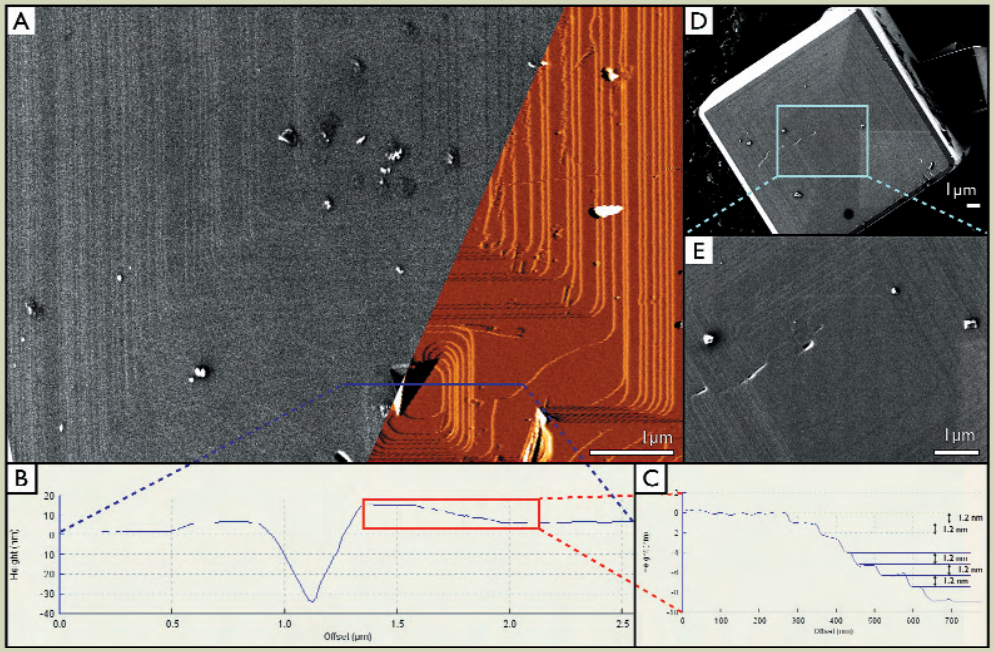

Fig.2 (A) composite HRSEM (left, grayscale) and AFM (right, red-scale) image of the exact same (100) surface of the exact same crystal of zeolite LTA. (B) Cross section is of AFM height measurements corresponding to the purple line with a zoom in (C). (D) whole (100) surface of zeolite LTA with a magnification of the position of prevailing screw dislocation in (E). HRSEM: 1 keV landing energy, 2.5 keV column energy, In-lens detector, Sb mode. AFM: Constant Force Mode.

not limited to the surface of the crystal but includes internal pore structure by cross section analyses - the three dimension structural information of which differs from the projected images observed in TEM. As most porous crystals are insulators, they are therefore subject to charging which reduces image information. Using extremely low landing energies* by a deceleration of highly unstigmated electrons leaving the objective lens called *gentle beam* (also known as *stage bias* or *retarding field*), we are able to remove charging whilst maintaining a finely focused electron probe as electrons pass through the objective lens with the column energy. We then explore the other types of detectable contrast produced from electron irradiated samples by careful filtering and detection of emitted electrons based on their energy using an energy filter for secondary electrons called r-Filter and we show that compositional contrast is extremely useful in understanding the nature of these new and exciting materials.

Experimental, Results and Discussion, etc.:

Instrument & Electron Interaction Overview

An SEM is composed of a number of chambers. The first is a column filled with an electron source, apertures, scanning coils and lenses, down which an electron beam is first generated, accelerated, demagnified to a small electron *probe*, and then deflected in a raster fashion over the area to be imaged in the main chamber. The interaction between the impact electrons and the sample generates a number of different electrons such as *back scattered electrons* (BE), *secondary electrons* (SE) and Auger electrons and other emissions such as characteristic and Bremsstrahlung X-rays, visible light through elastic and inelastic scattering processes. Inelastically generated and emitted SEs are classified into two types called SE1 and SE2 which are produced within materials either directly from an incident (primary) electrons or from internally scattered electrons, respectively. Therefore SE1 produces a contrast highly dependant upon sample surface geometry and gives topographic information selectively, while SE2 comes from larger depth and volume than those of SE1, the contribution of SE2 to the image reduces topographic information. It is noteworthy that reduction of SE2 contribution to an image can be made only by reducing the landing energy. Characteristic X-rays, which are used for EDS and WDS measurements, give chemical information. Rutherford scattering of electrons involves high scattering angles of impact electrons, a detectable proportion of which are scattered through a large enough angle such that their resultant trajectory allows them to exit through the sample surface as BE. As Rutherford scattering is highly dependant upon the electrostatic potential of the sample atom nucleus, and therefore the atomic number, BE therefore provides compositional contrast . The electrons generated are collected by a scintillator or solid state detector and the signal is multiplied and delivered as a grayscale value, depending upon the intensity, to a viewing screen that is progressively scanning in synchronisation with the scanning beam. The result is an image of the crystal that may be saved to film or digital image file. All HRSEM images in this article were taken using a JEOL high-resolution scanning electron microscope fitted with in-lens detector, gentle beam, cold field emission electron source and EDS detector (JSM-7000F and JSM-7401F) installed at Stockholm University, Sweden.

More information about the type of interactions produced can be found both in reference [6] and throughout this article. We begin by examining topographic contrast.

*Landing voltage
=accelerating (column) voltage - stage-bias voltage

Level of Information/Resolution & Comparison With Atomic Force Microscopy

An elegant example of the power of imaging in HRSEM compared to AFM is shown in **Figure 1**. Part A shows a twinned crystal of zeolite LTA where each twin is of similar size and shape and considerably overlapped. Visualisation of this twin would not be possible in AFM owing to the steep sides of the crystal. In parts B and C, we increase the mag-

nification to two areas where the twins intersect each other. The AFM would not be able to probe into the sharp angle between these two surfaces owing to hindrance from the tip shape nor would it be able to image the macroporosity along the twin intersection. Surface steps are clearly visible in Figure 1B and C implying a high level of vertical resolution - the size of such features is quantified below.

As discussed in the introduction, SEM has, until recently, been unable to image surface terraces of nanoporous crystals which are essential to further the understanding of their growth with this information only reliably attained by AFM. The topographic sensitivity is so high that surface terraces on zeolite LTA of 1.2 nm are clearly observable in HRSEM images. We have confirmed this by imaging the surface of zeolite LTA *ibidem* (in the same place) using both AFM and HRSEM and overlaying the two images as shown in **Figure 2**A. It can be seen that the two images overlap with extremely good correlation and all the terraces visible in AFM are observable in the HRSEM image. Height cross-sections from the AFM (Figure 2.B and C) show that the step heights are all 1.2 nm and therefore the nominal vertical sensitivity is higher than the guaranteed lateral resolution of the microscope at this beam condition (1.5 nm).

HRSEM images can be collected much more rapidly and from a larger area by HRSEM than AFM, thus making the technique particularly efficient. Images may also be obtained at lower magnifications than that of the AFM and still the terrace information is conserved (Figure 2D and E). In AFM, the area to be scanned is limited by the range of the piezoelectric crystal used to move either the cantilever or the stage (depending on the type of AFM) which delineates, and therefore distorts the image at high displacement. The distortion in HRSEM is so slight that it can be neglected: in **Figure 3**, the left hand image is composed of four individual images of zeolite LTL with detailed surface terraces which match up well enough so that they join together seamlessly. The surface information is still conserved as in the three digital zooms shown in Figure 3 A2 to 3A4, across the length of the crystal.

AFM uses a physical probe, rather than a beam of electrons, that scans in raster fashion across the surface of the area to be observed. The tip is therefore prone to probe-tip dilation as can be seen in Figure 3B where the surface crater of zeolite LTL is imaged in both AFM (Figure 3B1) and SEM (Figure 3B2 to 3B3) and the appearance of terrace forking, the gap between each prong, is undetectable to the bulky AFM probe. The latter shows much more information about the crater detail. AFM does not perform well when the sample surface is far from orthogonal to the probe, such cases include when crystals have rounded surfaces as in silicalite-2 [7] or upon examining surfaces that intersect at obtuse angles.

As HRSEM is unable to measure vertical heights directly, AFM was used to confirm vertical resolution illustrating one advantage of AFM over SEM [8]. In terms of lateral resolution, however, HRSEM is the optimum technique. We now illustrate how this level of resolution and contrast is not just limited to surface features but also applicable to the internal structure of materials by first using a new sample preparation technique called cross-section polishing.

Cross-Section Polishing & Comparison With Transmission Electron Microscopy

Cross-section polishing uses a beam of accelerated argon ions to *polish* the material of interest. By placing a shield that is resistant to the argon ion beam on top of the material, this shield protects a portion of the material from the abrasive argon ion beam, and polishing occurs as shown in **Figure 4**. There is a high dependancy of attrition rate upon the angle between material and direction of the argon ion beam. As the rate of attrition is effectively zero when the surface of the material is parallel to the argon ion beam, a very flat cross section is therefore formed. It is free from contamination and damage associated with other types of polishing such as mechanical or chemical etching [9]. In the case of porous crystals, they are first embedded in a (preferably conductive) medium such as silver loaded epoxy or carbon glue before being polished. In

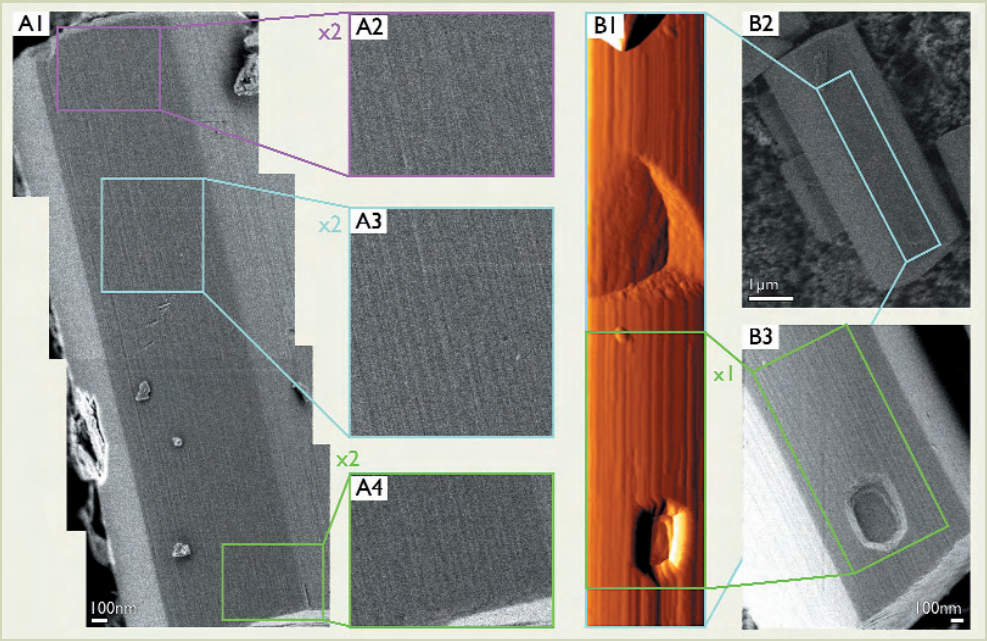

Fig.3 Zeolite LTL images. (A1) is a composite of four SEM images, the areas highlighted at the top (magenta - A2), middle (cyan - A3) and bottom (green - A4) of the crystal are 2x digital zoom of those images. Right hand crystal is shown in both AFM (B1), SEM (B2) and HRSEM (B3) images, notice the probe-tip dilation effect in the AFM reducing the amount of information around the small crater towards the bottom of the crystal. HRSEM: 0.8 keV landing energy, 2.3 keV column energy. In-lens detector, Sb mode. AFM: Constant Force Mode.

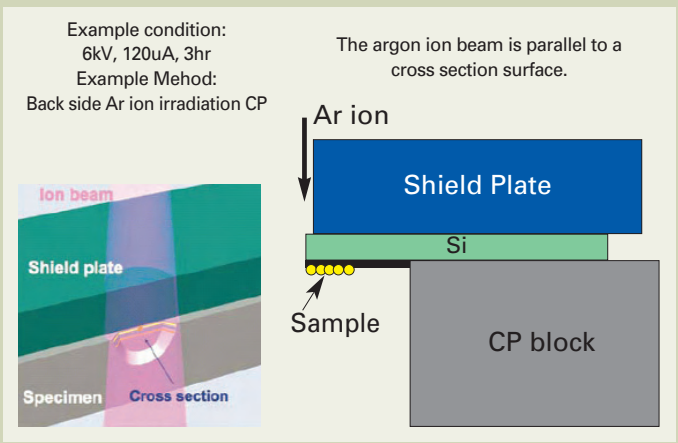

Fig.4 Schematic of the Cross Section Polisher as viewed from the side (top-right) and isometrically (bottom-left).

order to reduce imperfections in the etching process, the resin is heated or left under vacuum when drying in order to remove air bubbles, as these small cavities create eddies and fluctuations in the otherwise homogenous *stream* of the argon ion beam. It is noteworthy that much of the atrophied material produced in the polishing process presents enough of a volume to contribute to contamination contrast. To reduce this problem, the supports are cleaned with ethanol before sample preparation and heated to 250°C prior to introduction into the exchange chamber of the HRSEM.

In **Figure 5**, HRSEM images of SBA-15 are shown where the mesoporous channels terminate in corrugations on the side wall surface or as U-turns (Figure 5A) or open (Figure 5B) hexagonally distributed pores on the front wall. By encapsulating these crystals in a solid medium,it is possible to polish these materials as shown in Figure 5C to 5D. Once the internal structure is exposed it can be seen in the HRSEM that the polishing process is gentle enough to preserve both the mesoporosity and the interface between the different grains of SBA-15, the latter is invisible to TEM where the size of the crystal would be too thick for transmission and the lack of periodicity of the interface. Similarly, the change in orientation of the pore across an individual crystal can be followed. This point is reiterated in the spherical counterparts shown in both TEM (Figure 5F) and by cross section polishing (Figure 5E) where the contrast changes from lines (channels run perpendicular to the optic axis) to spots (channels run parallel). Cross-section polishing also allows a profile view of surface terminations that are visible in TEM but difficult to distingusih and disprove to be fracture lines of a crystal fragment caused by the compulsory crushing required to accommodate crystals of this size upon a TEM grid.

Gentle Beam Helps With Charging In Insulating Porous Materials

An unfortunate occurrence when imaging insulating specimens in HRSEM is that they often experience a phenomenon known as charging. This results in the masking of image information by areas of extremely high or low contrast or by a distortion in the image. This is due to a build-up of unstable and in-homogenous electric fields generated by either a net deficit or surplus of electrons provided by the impact electrons of the electron source which then leave the sample either by conduction to earth or by emission. These electric fields disrupt the trajectory and generation of emitted electrons. As most porous materials are composed of silica, they are virtually non-conductive and so balancing of electrons within the specimen requires tight control of the ratio of emitted to impact electrons, known as the electron yield, σ, preferably keeping it as close as possible to unity for a given beam condition. The electron yield varies greatly with both surface angle (thus giving rise to topographic contrast, as discussed above) and accelerating energy, or more precisely, the landing energy which is the energy electrons impact the surface of the sample. The critical energy and the general dependency of electron yield differs from material to material but follows a general curve with a negative gradient*. The landing energy may be controlled to find the *critical energy* which is the point below/above which the electron yield is respectively greater/less than unity [10]. In siliceous materials, this is usually between 500 eV and 1.5 keV. To highlight this we have imaged both SBA-16 and FDU-16; one silica based and the other carbon based, both of which possess the same structural symmetry and approximately the same pore density and shape. In **Figure 6**, where the contrast of each image is normalised against the highly ordered pyrolytic graphite (HOPG) substrate. As HOPG is very conductive and therefore has effectively a constant electron yield of 1 over all landing energy used. It can be seen in the case of SBA-16 that the critical energy is between 1.4 and 1.7 keV, whereas in FDU-16, the range is much larger and at relatively higher energies. Unfortunately for SBA-16, at the

*The function is actually hump shaped with a second, lower critical energy at a lower landing energy. As this side of the maxima (with a positive gradient) falls below the practical range of current microscopes, it is removed from the scope of this paper for pragmatic reasons.

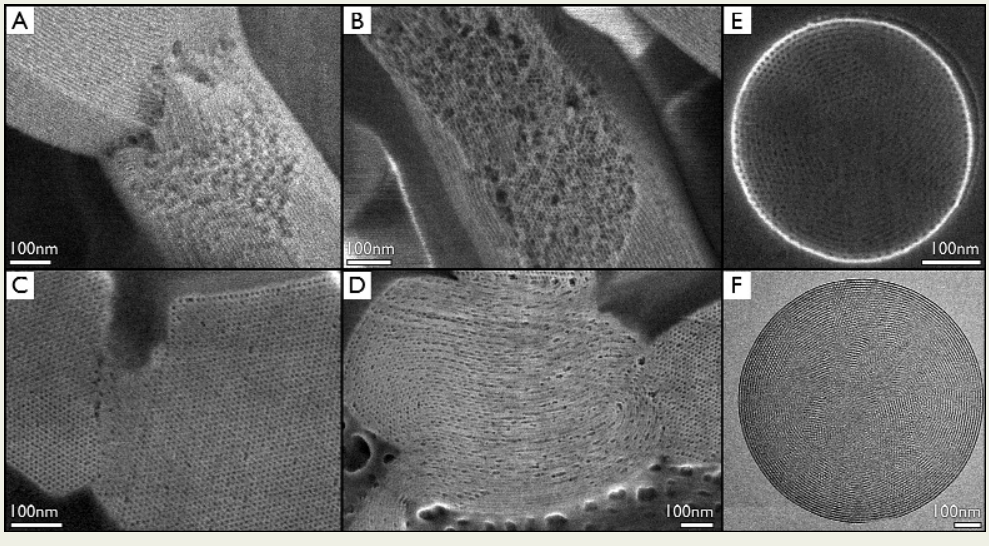

Fig.5 Mesoporous silica SBA-15. (A) and (B) are HRSEM images of the unaltered crystals clearly displaying surface channels and terminations. (C) and (D) are HRSEM of the powder after cross section polishing, notice surface profile is visible along with grain boundaries and change of channel orientation. (e) and (f) are of crystals with spherical morphology viewed both as a cross section (HRSEM) and projection (HRTEM), respectively.

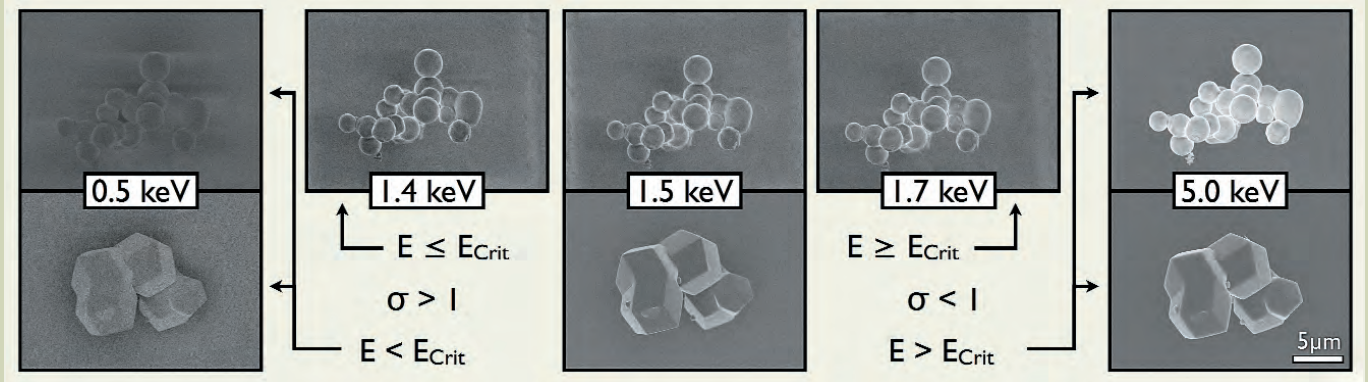

Fig.6 Mesoporous silica SBA-16 (top row) and reciprocal carbon analogue FDU-16 (bottom row) imaged at different accelerating voltages. Contrast normalized to that of the HOPG substrate. No surface bias. In-lens detector, Sb mode.

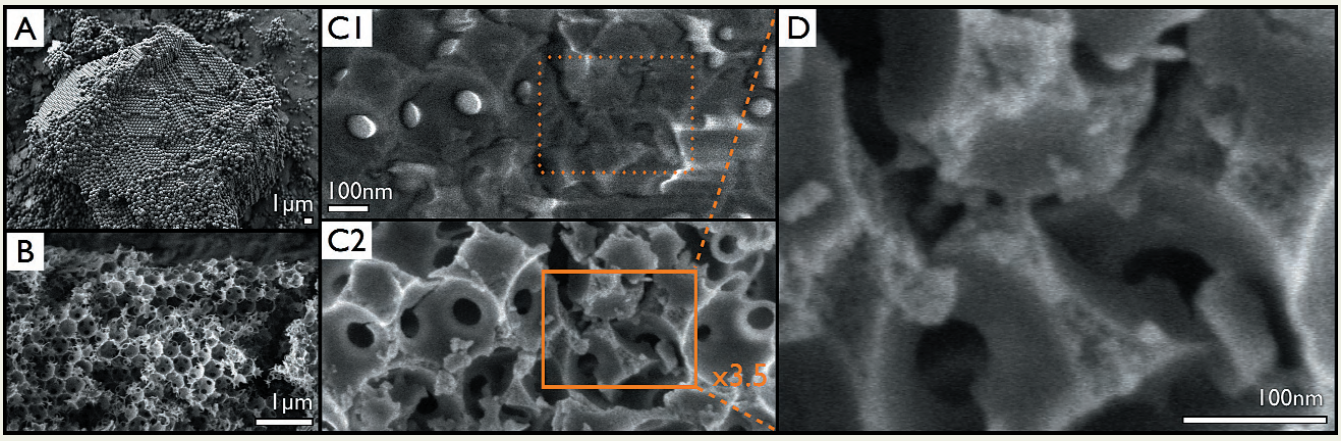

Fig.7 Hierarchical Porous Material. (A) polysterene spheres used to form macroporous template, (B) free powder, (C1) and (C2) taken without and with a 500 eV stage bias of the free powder lightly crushed exposing mesoporous network highlighted in(D). 3 keV column energy. In-lens detector, Sb mode.

range of desirable accelerating energies where charging is minimised, the diffraction error and chromatic aberration dramatically limit the minimum possible probe diameter and resolution drops below that required to image the important surface features [11].

To overcome the reduction in resolving power of the SEM at accelerating energies below 5 keV, the use of beam retardation, otherwise known as *gentle beam* mode, has been adopted. This is where the accelerating energy, which determines the minimum probe size and therefore the limit of the resolution when passing through the column (column energy), is retarded by a negatively charged stage bias to a lower, landing energy equal to the column energy minus the stage bias. The landing energy used is significantly lower than that used before in obtaining images of such high levels of resolution. Using this method it is possible to retain the advantage of high resolution imaging by having a high column energy but also reducing charging effects by operating at a lower landing energy.

A further benefit of gentle beam is that the electric field employed is orders of magnitude stronger, more homogenous and more stable than that of the small electric fields discussed above arising from sample surfaces with steep gradients or thin areas (i.e. tips and edges). This means that the stage bias supersedes the small fields and removes streaking and localised areas of charging, thus cancelling the disruption to the trajectory and energy of the emitted electrons. This can be seen in **Figure 7** where a hierarchical porous material [12] templated from polystyrene spheres (Figure 7A) is crushed producing many tips and edges. When imaged without and with a relatively small stage bias of 500 eV (Figure 7C1 to 7C2, respectively) the difference to the improvement of the contrast is striking. There is also an increased resolution that can be seen as the mesopores within the walls of the macropore owing to the higher column energy and the mesoporosity in the macroporous wall are now observable (Figure 7D).

Charging is just one way in which emitted electrons may lower the amount of information detected in an HRSEM image. By careful tuning of both the landing energy and the stage bias, it is possible to produce electrons with the maximum information desired by the user. We shall show in the next section how it is also possible to selectively tune the energy of emitted electrons and the corresponding information to be gleaned from such electrons.

r-Filter Used To Separate Different Types of Contrast

As discussed in the overview section, electrons with different energies, intensities and trajectories are generated during SEM dependant upon different factors. Fortunately, the energy difference between secondary and backscattered electrons is very large and SEMs fitted with an r-Filter are capable of independently detecting these different electrons. This is done by placing a detector not at the side of the SEM chamber but inside the objective lens. These *in-lens detectors* not only have a higher signal-to-noise ratio (as they are catching high-angle scattered electrons which are more prevalent when using gentle beam) but also facilitate the incorporation of electrodes placed in the objective lens which are then able to gate out/in electrons of different energies.

This can be seen in **Figure 8**, where Au@TiO_2 *rattlespheres* [13] are observed in *Sb mode* (predominantly secondary electrons, Figure 8.1A) where the information is topographic in nature, all electrons (Figure 8.1B) and *Bs mode* (predominantly back scattered electrons, Figure 8.1C) is almost all compositional contrast. By using both modes we are able to observe gold nanoparticles both encapsulated inside and outside the macroporous TiO_2 hollow spheres. The gold appears as bright spots of contrast in Bs mode. As can be seen in the images, both the short penetration of impact electrons with low landing energies and large attenuity of SE electrons allow for observation of gold particles on the surface of the spheres (Figure 8.2A to 8.2B) but is unable to distinguish other gold particles that are visible in the Bs mode appearing as very bright spots of contrast below the surface, encapsulated within the TiO_2 shell. The composition of both the shell and the nanoparticles with smaller than 20 nm in diameter are confirmed by now highly spatially resolved EDS measurements in spectra 2 and 1, respectively in Figure 8.3 - the same area is chemically mapped in Figure 8.4 for both titanium and gold.

Conclusion:

We have shown that HRSEM is a technique capable of extracting nanoscopic information both from the surface and inside nano-, meso- and macro porous materials. Such information is not readily accessible using other techniques such TEM and AFM. The information is maximized using a combination of technologies including; cross-section polishing; gentle beam and r-Filter. By using ultra-low landing energies whilst maintaining a highly stigmated electron probe we were able to produce images of extremely high resolution without charging masking the information. A more detailed account may be found in our upcoming review article [14].

Acknowledgments

The authors wish to acknowledge The Knut & Alice Wallenberg Foundation, Swedish Research Council, Japan Science and Technology Agency, EPSRC and ExxonMobil Research and Engineering for their financial support, JEOL SAS (Europe) and JEOL Ltd., for their technical support and Mohammad Jalil, Peter Alberius and L. Itzel Meza for supplying their samples. OT & YS acknowledge Prof. Kazuyuki Kuroda (Waseda University) for his continued encouragement and support.

References

[1] Yang et al. Revision of Charnell's procedure towards the synthesis of large and uniform crystals of zeolites A and X. *Microporous and Mesoporous Materials* **vol. 90 (1-3)** 53-61. (2006)

[2] Agger et al. Crystallization in Zeolite A Studied by Atomic Force Microscopy. *J. Am. Chem. Soc.* **vol. 120 (41)** 10754-10759. (1998) ; Sugiyama et al. AFM observation of double 4-rings on zeolite LTA crystals surface. *Microporous and Mesoporous Materials* **vol. 28 (1)** 1-7 (1999); Meza et al. Differentiating fundamental structural units during the dissolution of zeolite A. *Chemical Communications (Cambridge, United Kingdom)* **(24)** 2473-2475. (2007)

[3] Smaihi. Investigation of the Crystallization Stages of LTA-Type Zeolite by

Complementary Characterization Techniques. *European Journal of Inorganic Chemistry* **vol. 2003 (24)** 4370-4377. (2003)
[4] Che et al. Direct observation of 3D mesoporous structure by scanning electron microscopy (SEM): SBA-15 silica and CMK-5 carbon. *Angewandte Chemie* (International ed. in English) **vol. 42 (19)** 2182-5 (2003); Terasaki et al. Structural study of meso-porous materials by elecrron microscopy, "Mesoporous Crystals and Related Nano-Structured Materials", *Studies in Surface Science and Catalysis* **Vol. 148**, 261-288, Elsevier (2004);. Wakihara et al. Investigation of the surface structure of zeolite A. *Physical Chemistry Chemical Physics* **vol. 7 (19)** 3416-3418 (2005); Tueysuez et al. Direct imaging of surface topology and pore system of ordered mesoporous silica (MCM-41, SBA-15, and KIT-6) and nanocast metal oxides by high resolution scanning electron microscopy. *Journal of the American Chemical Society* **vol. 130 (34)** 11510-11517
[5] Terasaki. Electron Microscopy Studies in Molecular Sieve Science. *Molecular Sieves - Science and Technology* **vol. 2** 71-112 (1999)
[6] Reimer. Scanning Electron Microscopy. Berlin: Springer-Verlag (1998)
[7] Stevens et al. High-Resolution scanning electron and atomic force microscopies: observation of nanometer features on zeolite Surfaces. *Studies in Surface Science and Catalysis* **vol. 174 (2)** 775-780 (2008)
[8] Anderson Michael et al. Modern microscopy methods for the structural study of porous materials. *Chemical Communications* **(8)** 907-16 (2004)
[9] Erdman et al. Precise SEM cross section polishing via argon beam milling. Microscopy Today (2006) vol. May pp. 22-25; Takahashi et al. A New Method of Surface Preparation for High Spatial Resolution EPMA/SEM with an Argon Ion Beam. *Microchimica Acta* **vol. 155 (1-2)** 295-300 (2006)
[10] Cazaux. e-Induced secondary electron emission yield of insulators and charging effects. Nuclear Instruments & Methods in Physics Research, Section B: *Beam Interactions with Materials and Atoms* **vol. 244 (2)** 307-322 (2006); Rau et al. Second crossover energy of insulating materials using stationary electron beam under normal incidence. Nuclear Instruments and Methods in Physics Research Section B: *Beam Interactions with Materials and Atoms* **vol. 266 (5)** 719-729 (2008)
[11] Reimer. Image Formation in Low-Voltage Scanning Electron Microscopy. SPIE: Optical Engineering Press (1993); Mullerova and Frank. Scanning Low-Energy Electron Microscopy. *Advances In Imaging And Electron Physics* **vol. 128** 309-443 (2003)
[12] Loiola et al. Synthesis and characterization of hierarchical porous materials incorporating a cubic mesoporous phase. *Journal of Materials Chemistry vol.* **18 (41)** 4985-4993
[13] Schüth et al. To be published; Pablo M. Arnal et al. High-Temperature-Stable Catalysts by Hollow Sphere Encapsulation. *Angew. Chem. Int. Ed.* **45,** 8224-8227 (2006)
[14] Jansson et al. To be submitted.

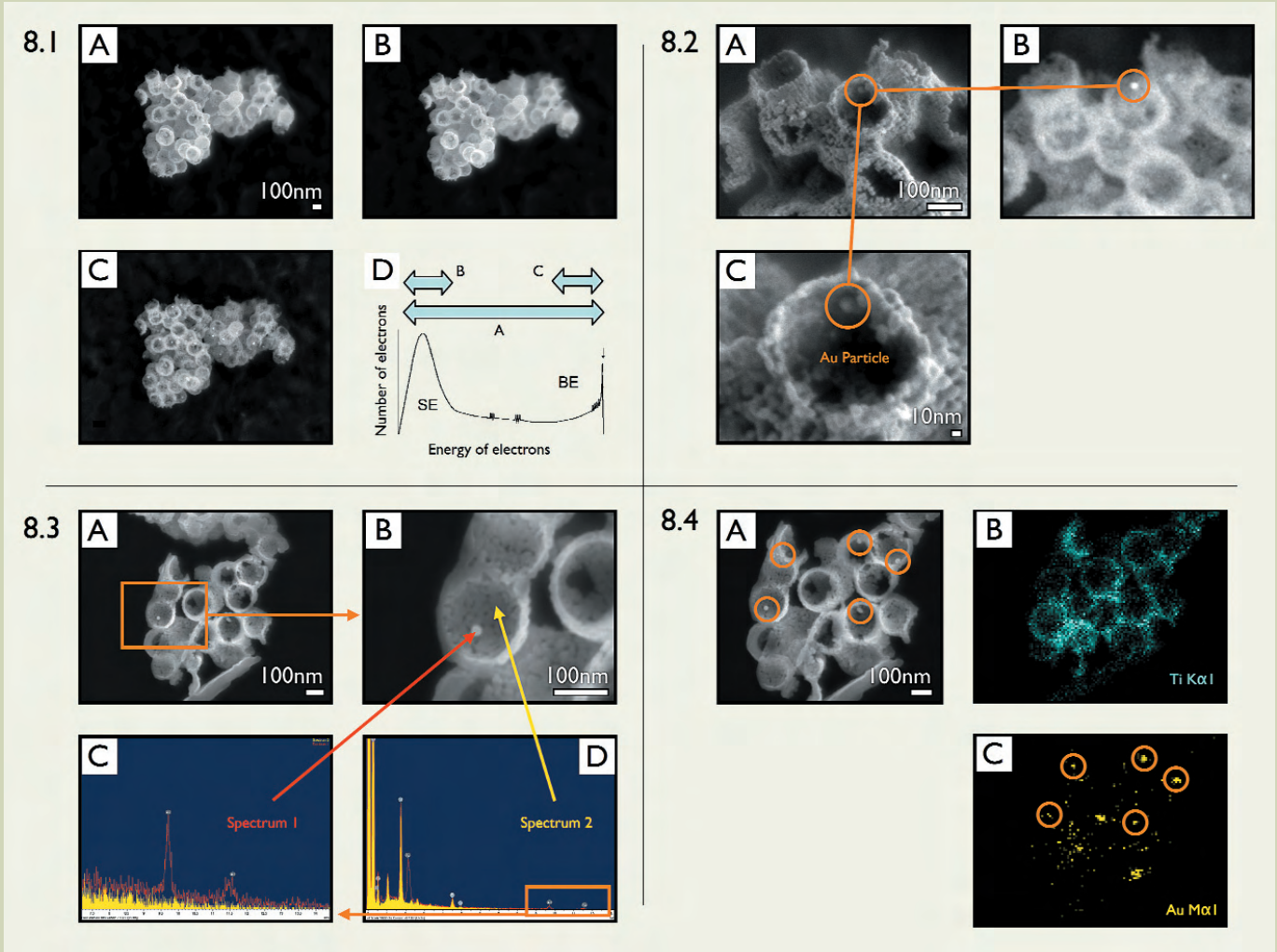

Fig.8.1 $Au@TiO_2$; Titanium nanoparticles creating interconnected macrospherical cavities, each encapsulating a gold nanoparticle. Images were taken at 3.0 kV with different ratios of SE (secondary) and BE (backscattered) electrons. Images constructed of only SE electrons (A), of a mixture of SE and BE electrons (Sb mode) using the r-Filter (B) and of only BE electrons (C).
8.2 A reduced landing energy of 500 eV (column energy 1.5 keV) produces topographical images (A and B) showing clearly the encapsulated gold (see as a compositional contrast change in top right image (C)- the position of the gold).
8.3 Confirmation, by EDS chemical analysis, of position of gold nanoparticle as found in Figure 8.2.
8.4 EDS mapping of spheres (A) showing titanium K-lines (B) and gold M-lines (C).